Mixing of a jet in a vortex wake under atmospheric stratification

Pierre Saulgeot, Vincent Brion, Nicolas Bonne, Laurent Jacquin, Emmanuel Dormy

Association Aéronautique et Astronautique de France

56th 3AF International Conference on Applied Aerodynamics
28 — 30 March 2022, Toulouse – France

FP64-AERO2022-Saulgeot

MIXING OF A JET IN A VORTEX WAKE UNDER ATMOSPHERIC STRATIFICATION

Pierre Saulgeot[(1)], Vincent Brion[(2)], Nicolas Bonne[(3)], Laurent Jacquin[(4)] and Emmanuel Dormy[(5)]

[(1)]*ONERA–DAAA, 8 rue des Vertugadins, 92190 Meudon, France, pierre.saulgeot@onera.fr*

[(2)]*ONERA–DAAA, 8 rue des Vertugadins, 92190 Meudon, France, vincent.brion@onera.fr*

[(3)]*ONERA–DMPE, 8 chemin de la Hunière, 91120 Palaiseau, France, nicolas.bonne@onera.fr*

[(4)]*ONERA–DSG, 8 chemin de la Hunière, 91120 Palaiseau, France, laurent.jacquin@onera.fr*

[(5)]*ENS–DMA, 45 rue d'Ulm, 75015 Paris, France, emmanuel.dormy@ens.fr*

ABSTRACT

A two-dimensional DNS is used to investigate the influence of atmospheric stratification and the relative position of the jets to the wake vortices on the distribution of the engine plume during its evolution in the vortex phase. A Boussinesq approximation is used and the engine plume is modelled as a passive scalar, without phase change. A wide range of Brunt-Väisälä frequencies and jet positions are studied. It is shown that these two parameters have a strong impact on the plume position over time. For certain stratification values, a secondary wake above the main wake oval is created and carries away all or part of the plume. In this regime, the jet-vortex distance has a major impact on the amount of plume carried into the secondary wake. If the plume is initially close to the vortex it remains in the primary wake oval, and if it is far from the vortex it is very quickly entrained in the secondary wake which rises to the flight altitude.

1. INTRODUCTION

Aircraft-generated contrails, which can evolve into artificial cirrus clouds (see fig. 1 (b)), constitute an important issue for both military aircraft (stealth) and civil aircraft (impact on the earth radiation balance, see [20]). These trails form under conditions of pressure, temperature and humidity (see [18]) that are often encountered at cruise altitude. Water vapour emitted by the engines comes on top of that contained in the atmosphere (see [30]), and may transform into ice by condensation (see fig. 1 (a)). In ice-saturated regions of the atmosphere, contrails can last several hours and degenerate into high-level cirrus

Figure 1: (a) Condensation behind jet engines. (b) Artificial cirrus due to contrails.

clouds. These have both cooling – reflection of solar radiation – and warming – reflection of infrared radiation from the earth – effects, the nocturnal effect causing warming. Recent studies [20] suggest that the impact of contrails could be larger than that of carbon dioxyde emission. Their radiative forcing may be dominant, accounting for more than half of the radiative forcing of civil aviation, while carbon dioxide accounts for only one third. However, the uncertainty on this measure is very high, as estimates range from 30 to 170%.

Immediately after its release into the atmosphere, the engine jets evolve under their own dynamics, mostly independent of the aircraft wake. It then follows an isobaric evolution, and the thermodynamic state (T, p_v) of any point of the jet is then located on the straight line passing through $(T_e, p_{v,e})$ and $(T_a, p_{v,a})$, respectively the thermodynamic conditions of the ambient atmosphere and jet. The slope of the jet mixing is given by

$$G = \frac{c_p p_a \mathrm{EI}_w}{(M_w/M_a) Q_{\mathrm{fuel}} (1-\eta)}. \qquad (1)$$

In this relation $c_p = 1\,004\,\mathrm{J\,kg^{-1}\,K^{-1}}$ is the specific heat capacity of air, p_a the pressure of the ambient atmosphere, $\mathrm{EI}_w = 1.23$ the engine vapor emission index

Variable	Significance
x	Horizontal coordinates
z	Vertical coordinate
b	Vortex spacing (time dependant)
b_0	Initial vortex spacing
z_0	Initial altitude
r_{jet}	Initial jet plume radius
b_{jet}	Initial jet plume spacing
z_{jet}	Initial jet plume altitude
z_{plume}	Plume altitude
Γ	Vortex circulation (time dependant)
Γ_0	Initial vortex circulation
r_0	Initial vortex core radius
W	Vertical speed of vortices
W_0	Initial vertical speed of vortices
N	Brunt-Väisälä frequency
$\bar{N}$	Scaled Brunt-Väisälä frequency
u	Fluid velocity
ω	Fluid vorticity
p	Pressure
p_v	Partial pressure of water vapor
q	Specific humidity
p^w_{sat}	Water vapour saturation pressure
p^i_{sat}	Ice vapour saturation pressure
ρ	Density
ρ_v	Partial density of water vapor
T	Temperature
θ	Potential temperature
Re	Reynolds number
Pr	Prandtl number
Sc	Schmidt number
Fr	Froude number
M	Mach number
A_j	Cross-sectional area of the jet
ρ_j	Jet density behind the engine
ϕ_j	Diameter of the jet behind the engine
R_d	Perfect gas constant for dry air
R_v	Perfect gas constant for water vapour

Table 1: List of variables

for conventional kerosene – 8.94 for liquid hydrogen, $(M_w/M_a) = 0.622$ the ratio of molecular masses of water and air, $Q_{\text{fuel}} = 43.2\,\text{MJ}\,\text{kg}^{-1}$ the fuel combustion heat for conventional kerosene – $120\,\text{MJ}\,\text{kg}^{-1}$ for liquid hydrogen – and $\eta = 0.3$ the overall propulsion efficiency of the aircraft at cruise (see [31]). By comparing this mixing line with the saturation vapour pressure curve of water, a criterion for the appearance of contrails, known as Schmidt-Appleman criterion, can be defined (see [1]). Comparison with the saturation vapour pressure curve of ice – lower than that of water in atmospheric conditions during cruise flight – allows the definition of a persistence criterion (see [29]). This criterion is illustrated in fig. 2.

Four phases can be distinguished in the evolution of the wake and engine jets in the atmosphere (see [6]): the jet phase, the vortex phase, the dissipation phase and the diffusion phase. Fig. 3 shows the first two phases, the second of which is of greatest interest here. The separation between these different phases is not strict. Qualitatively, the jet regime corresponds to the initial phase in which the jet has strong axial momentum (parallel to the plane motion), but this decreases rapidly. Generally the transition from the jet phase to the vortex phase is considered to have taken place when the jet dynamics has decreased very sharply and can be neglected. It can be described using the ratio R_3 introduced in [15] of the axial momentum to the transverse momentum of the jet:

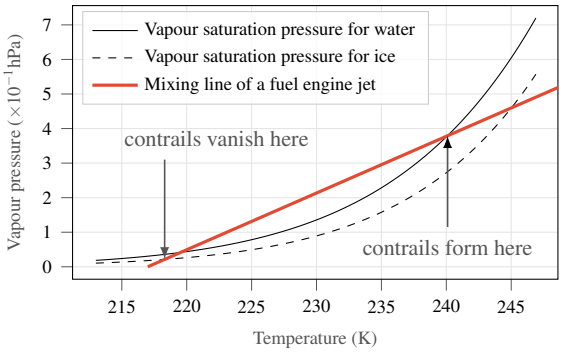

Figure 2: Illustration of the Schmidt-Appleman criterion for aircraft contrails. We use Goff-Gratch equations (see [9]) for the vapour saturation pression formulas.

$$R_3 = \frac{\Delta \mathfrak{p}}{\rho_0 V_\theta^2 A_j} = 16\pi \frac{\Delta \mathfrak{p}}{\rho_0 \Gamma_0^2} \left(\frac{r(x)}{D(x)} \right)^2 . \qquad (2)$$

In this relation $A_j = \frac{\pi D(x)^2}{4}$ is the cross-sectional area of the jet at a distance x downstream of the engine outlet. The jet is located at a distance $r(x)$ from the centre of the vortex, far enough away to consider that the flow due to the vortex is potential, *i.e.* $V_\theta(r) = \frac{\Gamma_0}{2\pi r}$. A semi-empirical law for D is given by $D(x) = a_D x$ with a_D of order 10^{-1} (see [24]). Jets produce a nominal thrust intensity $\mathfrak{p} = \rho_j U_j^2 A_j(0)$ where $A_j(0) = \frac{\pi \phi_j^2}{4}$, ϕ_j is the initial diameter of the jet and U_j the engine jet velocity. Cruising flight is characterised by the equality of thrust and drag. The increment of momentum flow induced by the engine whose flow is fed upstream by the external flow U_0 is $\Delta \mathfrak{p} = \rho_j U_j (U_j - U_0) A_j(0)$. A justification for the existence of the jet regime is given by $R(0) \gg 1$. The transition takes place for the length x_{jet} downstream of the jet such that $R_3(x_{\text{jet}}) \sim 1$. Taking the values corresponding to an A-330 (see [15]) we obtain $x_{\text{jet}}/b_0 \simeq 3.7$.

At this point, the wake vortices, generated by the rolling up of the vortex sheet issued by the aircraft various lifting surfaces, have already formed and are beginning to entrain the jets plume into their velocity field. Atmospheric effects also start to play an important role: stratification, wind shear, turbulence. The physics of the realistic flow remains to be fully understood. Free of turbulence and stratification, vortices descend throughout the atmosphere by induction of about half a dozen

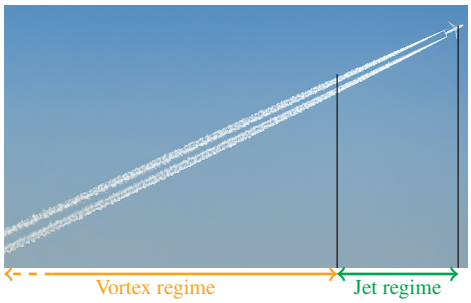

Figure 3: The first two regimes of the jets.

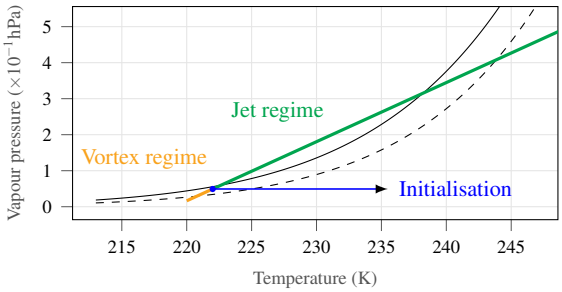

Figure 4: Schematic representation of the first two regimes on the dilution line. We initialize the study at the beginning of the vortex phase. For legend see fig. 3.

wingspans. After that, instabilities (most likely the Crow [3] or the elliptical [19] instabilities) will develop, giving rise to a succession of non-linear mechanisms that will eventually lead to the total loss of coherence of the flow and the dissipation of the wake momentum. High levels of turbulence accelerate the dissipation and bypass the Crow mechanism by strong transient dynamical processes (see [4]). The thermal stratification of the atmosphere modifies the vertical momentum of the vortices by buoyancy effect and baroclinic torque, which can significantly transform the vertical dynamics of the flow.

The question of the jet mixing in such a stratified environment especially requires further inquiry, as we do here. We review associated work thereafter. The dynamics of the engine jets and of the vortex sheet roll-up was the subject of a numerical study [5] and a wind tunnel experiment [17] to describe the influence of the position and temperature of the jets on the position of the plume in the near field. The work of [16] then focused on the persistence of wake vortices. The entrainment of jets in these vortices during the vortex phase was then analysed in [2] using a laminar numerical simulation. Several authors (for instance [6, 22, 21, 23, 34]) added the consideration of atmospheric conditions – stratification, wind shear, turbulence. In particular, stratification has been shown to have an important influence on the dynamic evolution of the wake, in particular the creation of the secondary wake. Turbulence can destabilise the vortices and cause instabilities to appear which dissipate them.

In this study, we investigate the role of stratification and jet engine lateral distance on the evolution of the jet plume in the vortex phase. Figure 4 shows that most of the dilution takes place during the jet phase and follows the straight line of slope G (eq. (1)). The end of the dilution takes place during the vortex phase. The wake then interacts with the atmosphere and the curve may change. The phenomena at play during this phase can then favour or hinder the appearance and persistence of contrails. The vortex wake is considered to be two parallel horizontal vortices and the plume is considered to be two passive scalar distributions moving, deforming and diluting under the wake influence. The Earth atmosphere is naturally stratified in temperature and the saturation vapour pressure varies with it. Thus it is important to know the position of the plume in order to determine whether a condensation trail might appear and persist. The value of the atmospheric stratification is therefore of great importance in the study of contrails. The position of engine jets in the wake of the aircraft has been little studied. However, it is an important parameter with regard to the plume lift and its evolution in the wake when it interacts with the atmosphere. Several simulations were therefore carried out for several initial length b_{jet} between the two initial plume disks. The initial altitude of the plume was not changed except for the case where we merged the centre of the discs with the centre of the vortices (simulation called "core").

2. FLOW MODEL

2.1 Flow and fluid description

At the beginning of the vortex phase the dynamic is mainly two dimensionnal and can be studied in the reference frame of the atmosphere at rest in a plane perpendicular to the direction of flight of the aircraft. In this plane, the wake is initially composed of two counter rotative Lamb-Oseen vortices of radius r_0 resulting from the roll-up of the vorticity sheet created by the lifting surfaces (according to the lifting line theory, see [27]). If we denote by b_a the wingspan of the aricraft, the reference lenth scale is the initial distance between the vortices $b_0 = \frac{4}{\pi} b_a$ and the reference time scale $\tau_0 = 2\pi b_0^2/\Gamma_0$ (see fig. 5). The engine plume is considered as a passive scalar with a regular initial axisymmetric distribution of radius r_j (see [22]). The dynamics of the engine jets during the jet phase is very turbulent, leading to a very strong dilution of the plume at the end of this phase: less than ten wingspans behind the aircraft, the temperature of the jet is only a few degrees higher than that of the ambient atmosphere (see [17]).

The fluid is a mixture of dry air and water vapour. Hereafter, the subscripts "d" and "v" are used to designate the quantities associated with each, while the absence of a subscript designates the mixture. The purpose

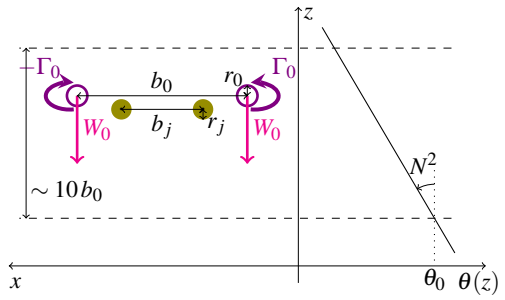

Figure 5: Model of the vortex and jet wake that initialize the vortex regime, and atmospheric conditions characterised by the Brunt-Väisälä frequency.

is to create a simple model of the influence of the parameters on the plume height. Therefore, phase changes are not taken into account and the plume is considered to be a single species. Dry air and water vapour are modelled as perfect gases in thermodynamic equilibrium. The equations of state are $p_d = \rho_d R_d T$ and $p_v = \rho_v R_v T$ for the partial pressures, where $R_d = 287\,\mathrm{J\,K^{-1}\,kg^{-1}}$ and $R_v = 461\,\mathrm{J\,K^{-1}\,kg^{-1}}$ are the respective perfect gas constants. The mixture also behaves like a perfect gas whose state depends on the specific humidity $q = \rho_v/\rho$. We then have $\rho_d = (1-q)\rho$ and $\rho_v = q\rho$. The pressure of the mixture yelds

$$p = p_d + p_v = \rho R_d T(1+\beta q) \tag{3}$$

where $\beta = \frac{R_v - R_d}{R_d} = 0.608$. Typical water vapor content in the atmosphere is less than 1% in mass. Humidity is most commonly given in terms of relative humidity $RH = 100\,p_v/p^w_{sat}$ where p^w_{sat} is the water partial vapor pressure at saturation (see [26]), a quantity which depends upon the temperature. Various empirical formula exist to relate saturation pressure and temperature. Here Goff-Gratch formulas (see [9]) valid for temperature from $-60\,^\circ\mathrm{C}$ to $102\,^\circ\mathrm{C}$ for liquid water and from $-100\,^\circ\mathrm{C}$ to $0\,^\circ\mathrm{C}$ for ice are chosen. A relation between RH and q is derived by first remarking that $q \simeq 0.622 p_v/p$ since q is small and then using the definition of relative humidity

$$q = 0.622\frac{RH}{100}\frac{p_{sat}}{p}. \tag{4}$$

At hight altitude atmospheric condition, $p \simeq 200\,\mathrm{hPa}$, $p_{sat} \simeq 5\,\mathrm{Pa}$ and, for instance, a relative humidity of 100% will give a specific humidity $q = 10^{-4}$. The humidity of the air therefore has a negligible influence on the dynamics.

2.2 Stratification

Stratification is taken into account using the Boussinesq approximation of the Navier-Stokes equations. The Boussinesq approximation consists in decomposing each of the variables of pressure, temperature, density and potential temperature as the sum of a reference value, a value varying slowly with altitude and a small perturbation due to the flow:

$$a(x,t) = a_0 + a_1(z) + a'(x,t). \tag{5}$$

The potential temperature is the temperature corrected for and adiabatic evolution, defined by $\theta = T\left(\frac{p_0}{p}\right)^{R/c_p}$, where R is the perfect gas constant and c_p the heat capacity at constant pressure of ambient air. The values of θ_0, $\theta_1(z)$, p_0 and $p_1(z)$ are equal to temperature and pressure of an adiabatic atmosphere, at flight altitude.

We call N the Brunt-Väisälä frequency defined by

$$N = \sqrt{\frac{g}{\theta_0}\frac{\mathrm{d}\,\theta_1}{\mathrm{d}\,z}}. \tag{6}$$

When $N = 0$, the thermal (and thus density) gradient is zero. The atmosphere is then said to be adiabatic. A positive value of N corresponds to a stably stratified atmosphere in which case a vertically displaced air parcel returns to its initial position by oscillating vertically at the frequency N. Negative values of N which correspond to an unstable stratification are not considered here.

The Boussinesq approach has been extensively used in the past to analyze the effect of stratification on wake vortices. A numerical simulation of laminar and two-dimensional vortex pairs at moderate Reynolds numbers was performed in [32] to evaluate the influence of stratification on the vortex evolution (see also [10, 25, 11]). The global scenario of the evolution of wake vortices under stable stratification is thus rather well described (see [14]). Stratification induces the formation of secondary vorticity at the interface between the oval containing the vortices and the surrounding atmosphere, by buyoancy and barocline effects. During this evolution, the vortices are seen to accelerate downward and approach each other, although there appears to be conflicting results on this point. For instance [28] finds, using experimental results, that the descent speed is reduced until finally turbulence, self instability and bursting diffuse the vortices. More recent works have been looking into the effect of three-dimensional structures and turbulence on this scenario. While during the early development of the wake the evolution is identical to that given by two-dimensional predictions, as [12] shows, the subsequent stages differ significantly, with the formation of coherent structures, and the accelerated inception of instabilities.

Stratification has an important impact on the vortex dynamics. This can be assessed by comparing the time scales associated with inertia and buyoancy. Vortices are driven by their descending velocity W_0 , an approximation of which is readily obtained using a point vortex model: $W_0 = \frac{\Gamma_0}{2\pi b_0}$. The Brunt-Vaisala frequency $\bar{N}$

Variable	Value	App. value	Reference
r_{jet}/b_0	$\frac{0.032}{\pi}$	0.01	[23]
b_{jet}/b_0	$\frac{0.32}{\pi}$ to $\frac{4}{\pi}$	0.1 to 1.3	
z_{jet}/b_0	$-\frac{0.324}{\pi}$ or 0 [a]	-0.1	[23]
r_0/b_0	$\frac{0.2}{\pi}$	0.064	[8]
$\bar{N}$	0 to 2		
Re	10^4		
Pr	0.7		[35]
Sc	1.3		[35]

[a] For $b_{\text{jet}} = b_0$ (the vortices and the plumes centers are identical).

Table 2: Values of the different parameters of the study

normalized on b_0 and W_0 comes out as the driving parameter of the dynamics, that we will refer to as the stratification parameter in the following $\bar{N} = N\tau_0$ where $\tau_0 = \frac{b_0}{W_0} = \frac{2\pi b_0^2}{\Gamma_0}$ is the inertial time scale of the flow. When $\bar{N}$ is low, the flow behaves as if it was in a homogeneous fluid. For value close to unity, the momentum of the vortex pair and buyoancy are of equal strength and strong modifications of the flow are to be expected.

Typically, the mean of N varies seasonally between 0.01 and 0.03 s^{-1} and τ_0 is between 30 s for a narrow-body airliner and 50 s for a wide one. $\bar{N}$ can therefore take values between 0.3 and 1.5.

2.3 Governing equations

The thermodynamic variables are scaled as follows:

$$\theta' = T_0 \,\text{Fr}^2\, \bar{\theta} \tag{7}$$

$$p' = \rho_0 W_0^2\, \bar{p}, \tag{8}$$

where $\text{Fr} = \frac{W_0}{\sqrt{g b_0}}$ is the Froude number. The Boussinesq approximation is valid under the following assumptions, which are all satisfied:

- the vertical scale of the flow is much smaller than the height of the atmosphere $b_0 \ll \theta_0 \left(\frac{\mathrm{d}\theta_1}{\mathrm{d}z}\right)^{-1}$ or put differently $\bar{N}^2\,\text{Fr}^2 \ll 1$ – in practice $\text{Fr}^2 \sim 2\times10^{-3}$ and $\bar{N}^2 = \mathscr{O}(1)$,
- the time scale of the flow is much larger than that of the acoustic waves which are therefore neglected and the Mach number of the flow is small so that $\text{M}^2 \ll \text{Fr}^2$ – in practice $\text{M}^2 = \frac{W_0^2}{\gamma R_d T_0} \sim 1\times10^{-5}$.

Writing the decomposition of eq. (5) for the different variables then gives the equations

$$\nabla\cdot\bar{u} = 0, \tag{9}$$

$$\frac{\mathrm{d}\bar{u}}{\mathrm{d}t} = -\nabla\bar{p} + \bar{\theta}e_z + \frac{1}{\text{Re}}\nabla^2\bar{u}, \tag{10}$$

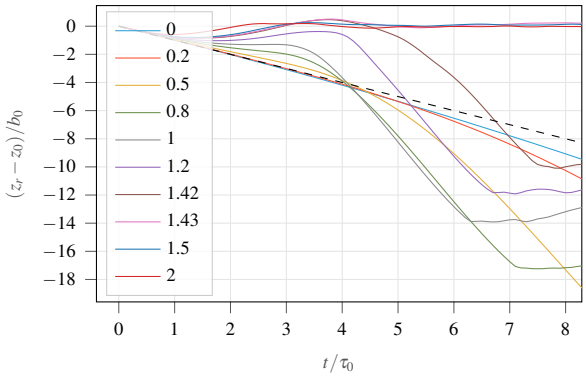

Figure 6: Altitude of the right vortex as a function of time for different values of $\bar{N}$, at $\text{Re} = 1\times10^4$. Black dotted line shows the equation $z = -t$.

$$\frac{\mathrm{d}\bar{\theta}}{\mathrm{d}t} = -\bar{N}^2\bar{u}\cdot e_z + \frac{1}{\text{Pr}\,\text{Re}}\nabla^2\bar{\theta}, \tag{11}$$

with $\text{Re} = \frac{W_0 b_0}{\nu}$, and $\text{Pr} = \frac{\nu}{k}$; time and space being scaled up (ν is the cinematic viscisity and k the conductivity).

The engine plume is considered to be water vapour. It is modelled by a passive scalar whose concentration $\bar{c}$ (scaled) follows a transport law

$$\frac{\mathrm{d}\bar{c}}{\mathrm{d}t} = \frac{1}{\text{Sc}\,\text{Re}}\nabla^2\bar{c} \tag{12}$$

where Sc is the Schmidt number.

A diagram of the initial flow, temperature, jet plume and stratification conditions is shown in fig. 5, and table 2 gives the values of the parameters. In particular, the initial jet plume distribution is the same as the temperature distribution, except for one multiplicative constant. This distribution is initialized by a tanh distribution, in accordance with [22].

2.4 Numerical procedure

The set of eqs. (9) to (12) is solved in a two-dimensional computational domain in laminar conditions using the code Nek5000. The coupled implicit linear system is solved for $\bar{u}$, $\bar{p}$ and $\bar{\theta}$ using spectral element multigrid to solve a Poisson equation for the pressure and then deriving the velocity. The computational domain for the flow solution is a rectangular box containing the two vortices and plumes. The horizontal dimension of the box is $L_x = 12b_0$ centered on the symmetry axis. The vertical dimension of the domain is $L_z = 24b_0$ and the position of the boundaries are adjusted depending on the stratification parameter. The domain comprises $N_x = 100$, $N_z = 200$ elements and $N_{GLL} = 12$ Gauss-Lobatto-Legendre points per element in each direction. The corresponding mesh resolution is determined by the largest separation between GLL points, *i.e.*

$$h_{max} \simeq \frac{\pi L}{2(N_{GLL}-1)N_e} \tag{13}$$

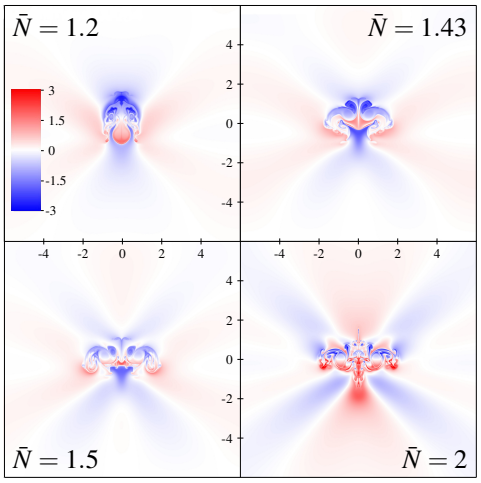

Figure 7: Perturbation temperature field at $t = 4\tau$ for different values of $\bar{N}$. The presence of gravity waves is clear.

In the current setup $h_{max} \simeq 0.017\, b_0$. Aliasing based on the two-third rule is used to increase the solver stability. The Boussinesq equations are advanced in time using a adaptative time step, which generates CFL ≤ 0.5. Symmetry boundary conditions are imposed on the left and right sides of the mesh, while the lower frontier is set with zero homogneous Dirichlet condition and the upper frontier with an outflow condition (zero condition for the pressure).

3. RESULTS

3.1 Description of the flow

The influence of stratification on the trajectory of the vortex pair is shown in fig. 6 over 8 characteristic time periods. The vortices initially descend by induction at speed $\bar{W}_0 = 1$. The downward motion of the vortex pair is then modified by the buyoancy forces scaled by $\bar{N}$. Buyoancy increases as the pair moves downstream and heats up by adiabatic compression. With increasing buyoancy the vortex pair first exhibits a rebound. Above $\bar{N} \simeq 1.43$ the vortex pair rebounds up to its initial altitude and stays aloft, with slight oscillations but no accelerated descent as before. This corresponds to the buyoancy forces being larger than the vertical momentum of the pair. Figure 7, which shows the temperature disturbance field for different $\bar{N}$ at $t = 4\tau$, highlights the gravity waves formed by these oscillations. An intermediate situation is observed from $\bar{N} = 0.5$ where the buoyancy force seems for a little time to be greater than the induction forces, before the ratio reverses again and an increased descent rate appears. For values of $\bar{N}$ between 0.8 and 1.42, it is observed that after a fairly long time ($\bar{t} \geq 6$) the descent of the wake is interrupted again. This is due to a disymmetrization phenomenon that will be studied in section 3.2.

The evolution of the total circulation in the flow is

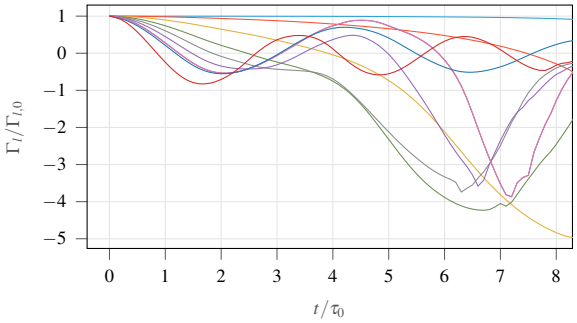

Figure 8: Ratio of total circulation (Γ_l) and initial circulation ($\Gamma_{l,0}$) on the left hand side of the domain as a function of time for different values of $\bar{N}$, at Re $= 1 \times 10^4$. For color legend see fig. 6.

shown in fig. 8. When $\bar{N} = 0$ the total circulation is conserved. The vortices remains unchanged for the duration of the computation. Momentum is almost conserved due to the low viscosity, and thus both circulation and vortex separation are constant.

However when buyoancy sets in, the reduction in vortex pair momentum is accompanied by a reduction of the circulation and by generation of opposite signed vorticity corresponding to the formation of a secondary wake above the primary vortices. This occurrence of secondary vorticity can be analyzed using the axial component of the vorticity equation (t et x are scaled)

$$\frac{\mathrm{d}\,\bar{\omega}}{\mathrm{d}t} = \frac{\partial \bar{\theta}}{\partial x} + \frac{1}{\mathrm{Re}} \nabla^2 \bar{\omega}. \tag{14}$$

The gradient of potential temperature at the Kelvin oval boundary caused by the presence of warm fluid inside and cold fluid outside (in the sense of potential temperature) leads to the emergence of a hot region at the top of the vortex pair characterized by opposite sign vorticity. Indeed, potential temperature gradient is positive and the fluid is colder at lower altitude, leading to warmer fluid in the descending oval than in the ambiant air. Circulation of opposite sign compared to the primary vortices builds up with time and overpass the initial vortex circulation at some point. The flow fields shown in figs. 9 and 10, using axial vorticity level plots, illustrate the development of the flow for two representative values of the buyoancy factor.

The flow for $\bar{N} = 1$ depicted in fig. 9 shows that the vortex pair retains most of its dynamics during its evolution. The formation of the secondary wake corresponds to a rebound of the pair, with a subsequent accelerated downward motion. At the same time the pair reduces in size and the vortices get closer. As the secondary vorticity form at the side of the oval, the vortices descent rate slows down: the induction of the secondary vorticity upon the primary vortices (by Biot-Savart) is directed vertically and upward. As a result of this action the vortices of the pair are subject to a reduction of their descent

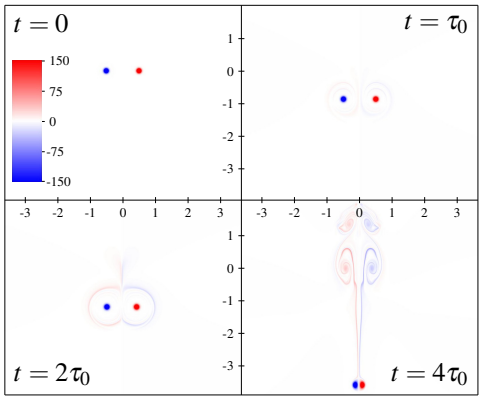

Figure 9: Evolution of the vorticity field for $\bar{N} = 1$ and $\mathrm{Re} = 1 \times 10^4$.

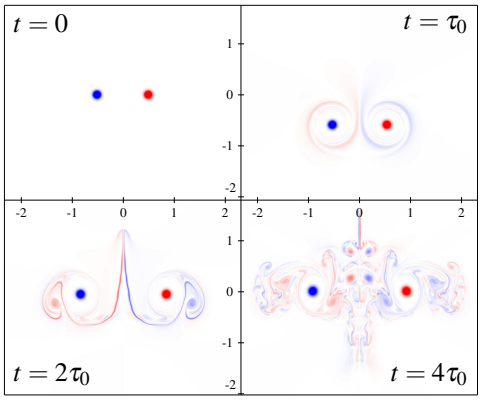

Figure 10: Evolution of the vorticity field for $\bar{N} = 2$ and $\mathrm{Re} = 1 \times 10^4$. For color map see fig. 9

velocity and can even move up, which is the case for instance when $\bar{N} = 1.2$ (see fig. 6). The vorticity present at the side of the vortex pair and induces the upward movement is also visible in fig. 9, $t = 2\tau_0$. When the secondary vorticity reaches the symmetry axis of the flow, the induction of the secondary vorticity upon the primary vortices is directed horizontally and inward. This time the vortices of the pair get closer to each other while keeping approximately a constant circulation and therefore accelerate downward at the subsequent stages. At such a close distance, strong vorticity cancellation occurs at the symmetry plane of the pair by viscous diffusion and the vortex pair descent acceleration increase, due to the increased induction. Once formed, the vorticity is progressively taken above the vortex pair along the oval upper boundary. This additional vorticity then accumulates above the vortex pair, and evolves under its self-induction. An increasing filamentation of its structure is observed. Such a behavior was already shown in [32] and [25]. In particular, [32] shows the same evolution of the vorticity field when $\bar{N} = 1$.

The flow for $\bar{N} = 2$ shown in fig. 10 indicates a dominant action of the buyoancy forces upon the vortex pair. The flow develops horizontally instead of vertically, with an oscillation of the vortices.

It is important to note that the two-dimensional constraint on the flow leads to an exagerated lifetime of the vortex pair. According to [33] the maximum lifetime of a vortex pair is about 5 to 6 characteristic times τ_0. Three-dimensional flow, if taken into account, would accelerate the deformations of the flow, notably through the development of instabilities and later, fine scale turbulence.

3.2 Disymetrization effects

As mentioned earlier, the interruption of the wake descent and the beginning of a slight rise for $t \geq 6\tau_0$ (depending on $\bar{N}$) is not due to an increase in lift compared to induction but to the appearance of a disymmetry in the primary wake which leads it to curve its descent trajectory, the rotation of one of the vortices starting to become more important than that of the other (see fig. 11). The disymmetry then propagates along the former axis of symmetry to the secondary wake. This phenomenon, which has been observed in the past, occurs when the wake descent is very rapid and the distance between the vortices has been greatly reduced. Two main explanations have been put forward. The first one (see [13]) considers that a Kelvin-Helmholtz instability forms at the boundary between the oval (warm in the sense of potential temperature) and the ambient air (colder and denser). The second one (see [14]) is that the vorticity sheet created at the boundary of the oval rather develops Taylor-Görtler instabilities. An explanation of this phenomenon by the collision of the two main vortices is also put forward in [7].

3.3 Dilution of the jet plume

The plume is drawn into the flow from its initial position in the Kelvin oval, beginning to wrap around the vortices, and is also subject to buoyancy. The influence of stratification on the average altitude of the plume is presented in fig. 13 over 8 characteristic times. Its position thus follows the initial descent of the vortices, independently of the stratification. The descent of the plume then slows down, like that of the eddies, but the final rebound seems to occur for a larger range of $\bar{N}$. Similarly, when the descent continues ($\bar{N} = 0.8$), it is quite weak and eventually comes to an end, and the plume rises again. There is even a late rebound of the plume to flight altitude ($\bar{N} = 0.5$), while the vortices descend very quickly after the rebound.

As for the vortices three situations can then be distinguished. For very small values of stratification ($\bar{N} \leq 0.2$) the plume follows the movement of the vortices and remains within the oval. When $\bar{N}$ is large enough for a secondary wake to form, the plume seems to be progressively drawn into it, ($\bar{N} \geq 0.5$). The situation for $\bar{N} = 0.5$ is a bit more peculiar: the plume remains in the oval for a long time before being drawn into the secondary wake.

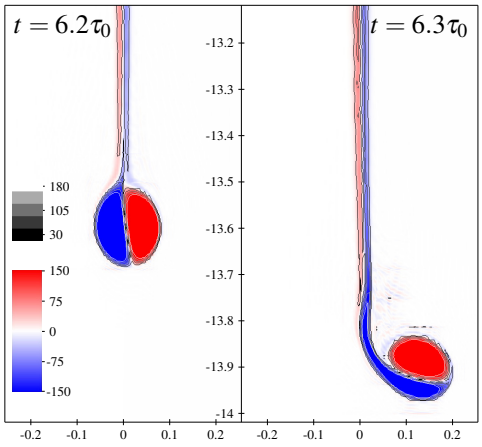

Figure 11: Detailed view of the vorticity field for $\bar{N} = 1$ and $\mathrm{Re} = 1 \times 10^4$ (contour: vorticity magnitude).

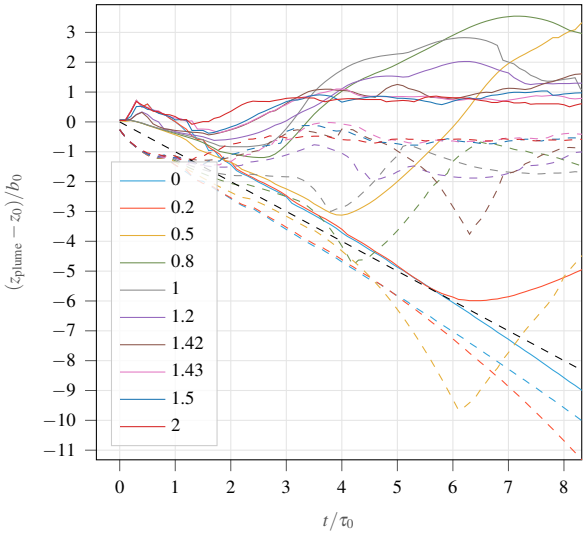

Figure 12: Maximum (plain) and minimum (dashed) altitude of the plume as a function of time for different values of $\bar{N}$, at $\mathrm{Re} = 1 \times 10^4$. Black dotted line shows the equation $z = -t$.

It should also be noted that an upward movement at the level of the axis of symmetry, which is formed as soon as a secondary wake appears, allows this constant ascent. As the stratification increases ($\bar{N} = 1.42$), the plume does not even begin to descend, it seems to be captured directly in the secondary wake. It is also worth noting that the trajectories are very similar for $\bar{N} = 1.42$ and $\bar{N} = 1.43$, while the dynamic behaviour is very different. In general, the coexistence of a primary and a secondary wake seems to favour the ascent of the plume, and this all the more so as $\bar{N}$ is large. Finally, when the stratification is too strong for the wake to descend beyond the initial movement ($\bar{N} \geq 1.43$), the plume remains at the flight altitude, as do the vortices.

The study of the impact of stratification on the altitude at which the minimum altitude part of the plume is located over time (see fig. 12) confirms this result in the

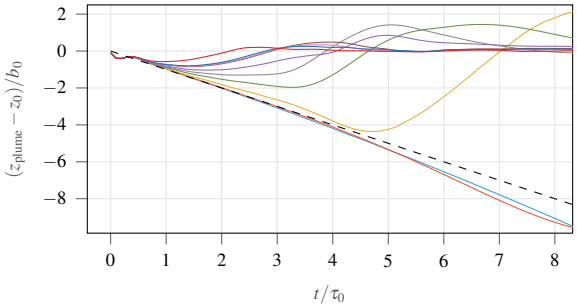

Figure 13: Mean altitude of the plume as a function of time for different values of $\bar{N}$, at $\mathrm{Re} = 1 \times 10^4$. For color legend see fig. 12.

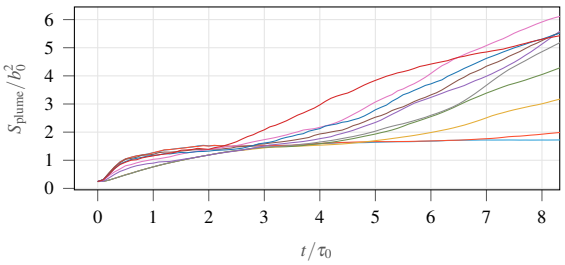

Figure 14: Surface of the plume as a function of time for different values of $\bar{N}$, at $\mathrm{Re} = 1 \times 10^4$. For color legend see fig. 12.

presence of two wakes. Indeed, for the smallest stratification values ($\bar{N} \leq 0.2$), there is always a part of the plume present at the altitude of the primary wake, thus in its oval. For $\bar{N}$ between 0.5 and 1.2, part of the plume also remains in the oval, but only for a certain time. Finally, this plot confirms that as soon as $\bar{N} = 1.42$ the whole plume is drawn into the secondary wake. Interesting information is also given in fig. 12 by the maximum altitude of plume elements: the secondary wake created for Brünt-Väisälä frequencies that allow it has a more extensive vertical structure than the main wake remaining at the flight altitude for higher frequencies. This results in a higher portion of the plume in the former case than in the latter. In particular, for $\bar{N} = 0.5$ to 1 or to a lesser extent 1.2, a portion of the plume is more than twice as high at a given time as for $\bar{N} \geq 1.43$. For $\bar{N} = 0.5$ or 0.8 this part of the plume remains at a high altitude. For $\bar{N} = 1$ or 1.2 the maximum altitude of the plume, however, then drops to values which are no longer much higher than those reached for a stronger stratification.

Eventually we look at the surface of the plume (see fig. 14). This makes it possible to measure the extent of the plume and to monitor the dilution of the water vapour. It is clear that the surface area increases faster the larger $\bar{N}$ is. This is due to the complex vortex structure that forms very early for high stratification values. However, spreading due to the large vertical extent of the secondary wake also plays an important role in the decrease of the concentration of passive scalar, although it appears for longer times. This is all the more true when the strat-

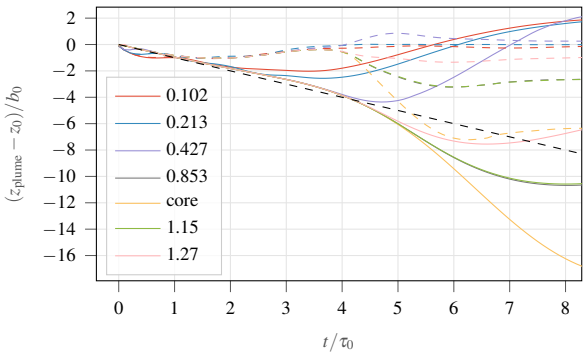

Figure 15: Mean altitude of the plume as a function of time for different values of b_{jet}/b_0, at $\text{Re} = 1 \times 10^4$. Solid lines represent $\bar{N} = 0.5$ and dashed ones $\bar{N} = 1.2$. Black dotted line shows the equation $z = -t$.

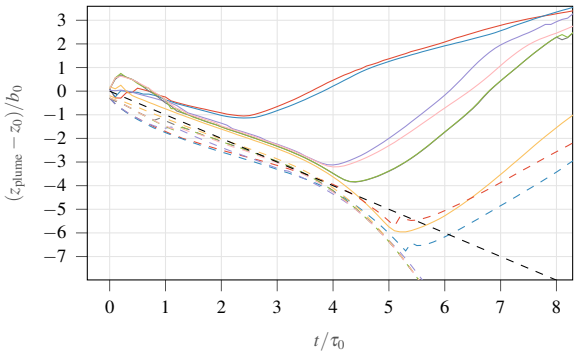

Figure 16: Maximum (plain) and minimum (dashed) altitude of the plume as a function of time for different values of b_{jet} at $\bar{N} = 0.5$ and $Re = 1 \times 10^4$. For color legend see fig. 15. Black dotted line shows the equation $z = -t$.

ification is important, and this phenomenon seems to be able to lead to a spread that exceeds the horizontal for times a little longer than the end of our simulation.

3.4 Effects of the jet-vortex distance

Figure 15 shows the temporal evolution of the mean plume altitude as a function of b_{jet} for two values of $\bar{N}$ in the intermediate regime where the vortex pair develops a secondary wake (0.5 and 1.2). It is clear that the closer the plume is to the vortices at the initial start, the more the plume descends. Indeed, in this case, it stays more in the oval and is less entrained in the secondary wake. These same effects can be seen in the plume end position curves (see fig. 16 for $\bar{N} = 0.5$).

In the case where the wake remains unique ($\bar{N} = 0$, $\bar{N} \geq 1.43$), the change in b_{jet} has no influence on the evolution of the plume altitude. Indeed, there is no vertical stretching and either the oval remains large ($\bar{N} = 0$) and contains the whole plume, or the wake remains at the flight altitude ($\bar{N} \geq 1.43$) and so does the plume, whatever its initial distance from the vortices.

4. CONCLUSION

Knowledge of the mechanisms of contrail formation and persistence is critical to the study of the radiation balance of civil aviation. In order to improve our understanding, it is necessary to know the spatial distribution of the vapour plume from engine jets. It is then possible to study its thermodynamic state and to deduce the dynamics of possible ice crystals, as the ambient air is warmer at lower altitudes. This study allowed us to better understand the influence of two parameters: atmospheric stratification and the initial position of the plume. We have determined that there are three regimes of evolution of the vortex wake of an aircraft as a function of stratification: either both wake vortices descend (little or no stratification), or a secondary wake is created and the descent rate of the primary wake increases, it eventually breaks up (intermediate stratification), or the primary wake remains at the flight altitude (strong stratification). We have seen that these three regimes lead to three plume evolution regimes. We have also observed that, under the second regime, the initial position of the plume has a strong influence on its interaction with the wake, and therefore its temporal evolution. The closer the plume is to the vortices at the initial time, the longer it remains in the primary wake oval. Thus, a plume emitted closer to the aircraft fuselage rises very quickly to flight altitude in the secondary wake and will not be able to warm up as it descends to a warmer atmosphere, unlike a plume emitted near the vortices. It would certainly make sense, with regards to contrails, to take this parameters into account in the design of new generation aircrafts.

REFERENCES

[1] H. Appleman. The formation of exhaust condensation trails by jet aircraft. *Bulletin of the American Meteorological Society*, 34(1):14 – 20, 1953.

[2] S. Brunet, F. Garnier, and L. Jacquin. Numerical/experimental simulation of exhaust jet mixing in wake vortex. *AIAA 30th Fluid Dynamics Conference*, 1999.

[3] S. C. Crow. Stability theory for a pair of trailing vortices. *AIAA Journal*, 8(12):2172–2179, 1970.

[4] S. C. Crow and E. R. Bate. Lifespan of trailing vortices in a turbulent atmosphere. *Journal of Aircraft*, 13(7):476–482, 1976.

[5] F. Garnier, S. Brunet, and L. Jacquin. Modelling exhaust plume mixing in the near field of an aircraft. *Annales Geophysicae*, 15(11):1468–1477, 1997.

[6] T. Gerz, T. Dürbeck, and P. Konopka. Transport and effective diffusion of aircraft emissions. *Journal*

of Geophysical Research, 103(D20):25905–25913, 1998.

[7] T. Gerz and F. Holzäpfel. Wing-tip vortices, turbulence, and the distribution of emissions. *AIAA Journal*, 37(10):1270–1276, 1999.

[8] T. Gerz, F. Holzäpfel, and D. Darracq. Commercial aircraft wake vortices. *Progress in Aerospace Sciences*, 38(3):181–208, 2002. ISSN 0376-0421.

[9] J. A. Goff. Low-pressure properties of water-from 160 to 212° F. *Trans. Am. Heat. Vent. Eng.*, 52:95–121, 1946.

[10] A. M. Hecht, A. J. Bilanin, and J. E. Hirsh. Turbulent trailing vortices in stratified fluids. *AIAA Journal*, 19(6):691–698, 1981.

[11] F. M. Hill. A numerical study of the descent of a vortex pair in a stably stratified atmosphere. *Journal of Fluid Mechanics*, 71(1):1–13, 1975.

[12] F. Holzäpfel, T. Gerz, and R. Baumann. The turbulent decay of trailing vortex pairs in stably stratified environments. *Aerospace Science and Technology*, 5:95–108, 2001.

[13] F. Holzäpfel and T. Gerz. Two-dimensional wake vortex simulations in the stably stratified atmosphere. *2nd AIAA, Theoretical Fluid Mechanics Meeting*, 1998.

[14] F. Holzäpfel and T. Gerz. Two-dimensional wake vortex physics in the stably stratified atmosphere. *Aerospace Science and Technology*, 3(5):261–270, 1999. ISSN 1270-9638.

[15] L. Jacquin and F. Garnier. On the dynamics of engine jets behind a transport aircraft. *ONERA-Publications-TP*, 1996.

[16] L. Jacquin and C. Pantano. On the persistence of trailing vortices. *Journal of Fluid Mechanics*, 471:159–168, 2002.

[17] L. Jacquin, *et al.* An experiment on jet-wake vortex interaction. *37th AIAA Fluid Dynamics Conference and Exhibit*, 2007.

[18] B. Kärcher. Formation and radiative forcing of contrail cirrus. *Nature communications*, 9(1):1–17, 2018.

[19] S. Le Dizès and L. Laporte. Theoretical predictions for the elliptical instability in a two-vortex flow. *Journal of Fluid Mechanics*, 471:169–201, 2002.

[20] D. S. Lee, *et al.* The contribution of global aviation to anthropogenic climate forcing for 2000 to 2018. *Atmospheric Environment*, 244, 2021.

[21] T. Misaka, *et al.* Vortex bursting and tracer transport of a counter-rotating vortex pair. *Physics of Fluids*, 24(2), 2012.

[22] R. Paoli, *et al.* Dynamics and mixing in jet/vortex interactions. *Physics of Fluids*, 15(7):1843–1860, 2003.

[23] R. Paoli, *et al.* Effects of jet/vortex interaction on contrail formation in supersaturated conditions. *Physics of Fluids*, 25(5), 2013.

[24] D. Papamoschou and A. Roshko. The compressible turbulent shear layer: an experimental study. *Journal of fluid Mechanics*, 197:453–477, 1988.

[25] R. E. Robins and D. P. Delisi. Numerical study of vertical shear and stratification effects on the evolution of a vortex pair. *AIAA Journal*, 28(4):661–669, 1990.

[26] R. R. Rogers. *A short course in cloud physics*. Pergamon Press Oxford ; New York, 1979.

[27] P. G. Saffman. *Vortex dynamics*. Cambridge university press, 1995.

[28] T. Sarpkaya. Trailing vortices in homogeneous and density-stratified media. *Journal of Fluid Mechanics*, 136:85–109, 1983.

[29] U. Schumann. On conditions for contrail formation from aircraft exhausts. *Meteorologische Zeitschrift*, 5:4–23, 1996.

[30] U. Schumann. Formation, properties and climatic effects of contrails. *Comptes Rendus Physique*, 6(4):549–565, 2005. ISSN 1631-0705.

[31] U. Schumann. A contrail cirrus prediction model. *Geoscientific Model Development*, 5(3):543–580, 2012.

[32] P. R. Spalart. On the motion of laminar wing wakes in a stratified fluid. *Journal of Fluid Mechanics*, 327:139–160, 1996.

[33] P. R. Spalart. Airplane trailing vortices. *Annual Review of Fluid Mechanics*, 30(1):107–138, 1998.

[34] S. Unterstrasser, *et al.* Dimension of aircraft exhaust plumes at cruise conditions: effect of wake vortices. *Atmospheric Chemistry and Physics*, 14(5):2713–2733, 2014.

[35] G. K. Vallis, D. J. Parker, and S. M. Tobias. A simple system for moist convection: the rainy–bénard model. *Journal of Fluid Mechanics*, 862:162–199, 2019.